
Article:
Zhou, L. orcid.org/0000-0001-7760-832X, Zhang, J. orcid.org/0000-0002-3354-0690, Zhang, J. orcid.org/0000-0003-3750-6841 et al. (1 more author) (2024) An environment-adaptive radio propagation path loss model with ray-based validation. IEEE Antennas and Wireless Propagation Letters, 23 (10). pp. 3217-3221. ISSN: 1536-1225

https://doi.org/10.1109/lawp.2024.3432578

An Environment-Adaptive Radio Propagation Path Loss Model with Ray-Based Validation

Lingyou Zhou, *Student Member, IEEE,* Jie Zhang, *Senior Member, IEEE,* Jiliang Zhang, *Senior Member, IEEE,* and Kehai Qiu, *Member, IEEE*

***Abstract*—In this letter, we introduce an adaptive multiple path loss exponent (AMPLE) radio propagation model considering environmental factors. The AMPLE model aims at predicting path loss with low computational complexity, while maintaining an acceptable prediction accuracy. Following that, we validate the model via Ranplan Professional simulations and compared it with the alpha-beta-gamma (ABG) and the 3rd Generation Partnership Project (3GPP) path loss models. The results show that the AMPLE model outperforms the path loss predictions of both the ABG and 3GPP path loss models.**

***Index Terms*—Path loss, prediction, radio propagation, ray tracing.**

I. Introduction

THE predictions of radio propagation path loss are significant tasks in large-scale parameters of channel modeling. In the fifth generation (5G) or beyond 5G (B5G), path loss models have been required to be simple, accurate, general, and moreover, potentially capable of covering environmental factors to cope with complex environments [1], [2].

Currently, one of the key categories for path loss prediction is the deterministic model based on ray optics. Along with detailed environmental information of the desired scenario, the deterministic models reveal precise propagation details, including path loss and other channel characteristics, by applying Maxwell's equations with appropriate boundary conditions [3]–[7]. However, they are quite complex when considering path loss only. They require comprehensive environmental data and involve high computational complexity, which makes them difficult to deploy across various propagation scenarios for path loss predictions. Conversely, for simplicity, empirical models use a small set of parameters to characterize path loss, which are constructed based on measurements under various scenarios [8], [9]. However, while these models are fast and simple, they are hard to cover different scenario types, and their prediction accuracy is largely sacrificed.

This work is funded by Innovate UK Project Radio Signal as a micro-Service (RSaaS). *(Corresponding author: Jie Zhang.)*

Lingyou Zhou is with the Department of Electronic and Electrical Engineering, The University of Sheffield, S10 2TN Sheffield, U.K., and also with Ranplan Wireless Network Design Ltd., CB23 3UY Cambridge, U.K.

Jie Zhang is with Ranplan Wireless Network Design Ltd., CB23 3UY Cambridge, UK, and also with the Department of Electronic and Electrical Engineering, The University of Sheffield, S10 2TN Sheffield, UK.

Jiliang Zhang is with College of Information Science and Engineering, Northeastern University, Shenyang 110819, China.

Kehai Qiu is with the Department of Computer Science and Technology, University of Cambridge, CB3 0FD Cambridge, U.K., and also with Research and Development, Ranplan Wireless Network Design LTD, CB23 3UY Cambridge, U.K.

This is the author accepted manuscript of an article published in IEEE Antennas and Wireless Propagation Letters. The final published version is available at https://doi.org/10.1109/LAWP.2024.3432578.

To generally predict path loss while maintaining both simplicity and accuracy, the geometry-based stochastic models (GBSMs) regress measurements and/or simulations under different scenarios and model shadow fading with log-normal distributions [10]–[18]. Typical path loss models that are widely used within those GBSMs include the close-in (CI) free space reference distance path loss model, CI model with frequency-dependent path loss exponent (CIF), and the alpha-beta-gamma (ABG) path loss model [18]–[20]. However, even though they cover different scenario types with the corresponding path loss models, without redesigning the model structure, those models cannot further develop with specific consideration of environments.

In this letter, we introduce AMPLE – an Adaptive Multiple Path Loss Exponent radio propagation model considering environments [21], [22]. For model validation, instead of relying on limited and truncated data points from measurements due to device sensitivity [21], we employ Ranplan Professional, a measurement-validated commercial ray tracing simulator [5]–[7], to verify the AMPLE model. The ray-based dataset helps overcome inaccurate characterization resulting from incomplete measurements by conducting comprehensive propagation simulations across the entire 3-dimensional (3D) simulated area, along with a 30-fold increase in data volume and complete path loss without truncations. In comparison with path loss prediction of the ABG and 3rd Generation Partnership Project (3GPP) models (as the extension of ABG model) [17], [18], the results show that the AMPLE model outperforms these two models by considering environments.

II. The AMPLE Model

In this section, we introduce the process of generating the AMPLE model. An example of the modeling process is shown in Fig. 1, including measurement and/or simulation scenario, environment recognition, model construction, and characterizations and predictions.

A. Propagation Scenario and Environment Recognition

For the scenario under consideration, the measurement and/or simulated data is collected first, which aims to regress and modify the parameters of the AMPLE model in the later stage. As shown in Fig. 1(a), the path loss results for an outdoor scenario is simulated by Ranplan Professional [6], [7] (reported in Section III), which contains the path loss between one transmitter (Tx) and Z receivers (Rxs) that are mapped across the whole area. Note that similar data formats (i.e., one Tx with Z Rxs) can be considered as alternatives for the case of measurement.

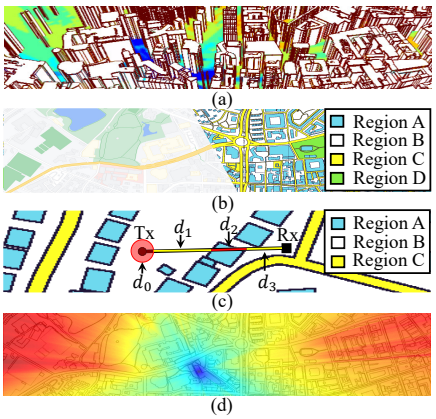

Fig. 1. Process of generating the AMPLE model. (a) Scenario with simulation/measurement. (b) Region classification. (c) Model construction method. (d) Path loss prediction.

To collect information of environments, we consider the 2-dimensional (2D) raster maps which contain different colors, shown as different red, green, and blue (RGB) values. By calculating the Euclidean distance between color RGB values with machine learning methods such as k-means clustering, the scenario can be classified into several region types (e.g., building as a region type). An example is shown in Fig. 1(b) (reported in Section III), the original raster map contains different colors (the left half of Fig. 1(b)), and, the map is recognized into four types of regions (i.e., Region A to D) based on the RGB values (the right half of Fig. 1(b)).

B. Model Construction

Initially, each region type is assigned a path loss exponent (PLE) to parameterize the environmental factors. To construct the model, a direct path between each Tx-Rx pair is generated, which records the intersected regions and the corresponding region lengths. Note that the direct path is irrelevant to the line-of-sight (LOS) path, since LOS may not happen for all links, and, it is just to construct the AMPLE model. The rationality of this simplified direct path is discussed in Section V. Since each region type is labeled with a PLE, that is, for the zth Tx-Rx pair, a path matrix $\mathbf{S}_z$ can be generated containing the intersected region PLEs and the region lengths, which can be expressed as

$$\mathbf{S}_z = \begin{bmatrix} n_0 & n_1 & n_2 & \cdots & n_{R_z} \\ d_0 & d_1 & d_2 & \cdots & d_{R_z} \end{bmatrix}, \tag{1}$$

where R_z is the number of intersected regions for the direct path of zth Tx-Rx pair, n_{R_z} is the R_zth intersected region PLE, and d_{R_z} is the corresponding region length. Besides, it should be noted that d_0 is the CI distance, and regions within length d_0 are not counted, which is referred to as the CI region in total. That is, n_0 is 0 where the path loss at d_0 is regressed as an intercept from simulations and/or measurements. An example is shown in Fig. 1(c), where three types of regions are classified, and the direct path intersects 3 regions (i.e., $R_z = 3$, and the CI region is not counted), along with the corresponding lengths from d_0 to d_3.

For the zth Tx-Rx pair with path matrix $\mathbf{S}_z$, the decibel path loss can be expressed as

$$PL_z = A + \sum_{r=1}^{R_z} 10 n_r \log_{10}\left(\frac{\sum_{k=0}^{r} d_k}{\sum_{k=0}^{r-1} d_k}\right) + p_z X + \Psi_\sigma, \tag{2}$$

where A, R_z, n_r, d_k, X, p_z and Ψ_σ are characterized as follows.

Intercept (A): For the direct path, A is the decibel path loss at CI distance d_0, which is data-derived.

Intersected Regions (R_z, n_r): For zth Tx-Rx pair, the direct path intersects R_z regions, and n_r is the PLE of rth region.

Weighted Distance (d_k): To compute the weighted path loss for the rth region, the weighted distance is computed first as the fraction in parentheses, where d_k is the kth region length. Note that the fraction under logarithms becomes a subtraction, yielding the weighted path loss of the desired region.

Penetrations (X, p_z): X is the penetration loss when the direct path intersects buildings, and p_z is the total number of penetrations in the path. When the path intersects a building, two penetrations are considered (i.e., in & out). We assume that penetrations will only occur for this region type (i.e., building), and p_z is zero if the building as a region type does not exist in the covered scenario.

Shadowing (Ψ_σ): Ψ_σ is normally distributed in dB scale with a zero mean and a standard deviation σ.

Equation (2) can be further simplified by combining terms with the same PLE. In other words, the AMPLE model can be computed with the region types that the path intersected, which is

$$PL_z = A + \sum_{m=1}^{M} D_m n_m + p_z X + \Psi_\sigma, \tag{3}$$

where M is the total number of region types that are classified from the environment (e.g., M is three in Fig.1(c)), n_m is the mth region type PLE, and D_m is the coefficient of n_m that is computed based on combining terms with the same PLE n_m in (2). Since Ψ_σ follows a normal distribution in decibels, the total path loss is therefore normally distributed with $N[\mu(A, n_m, X), \sigma^2]$, where

$$\mu(A, n_m, X) = A + \sum_{m=1}^{M} D_m n_m + p_z X. \tag{4}$$

Combining (2)-(4) with measured and/or simulated data, the parameters that construct the model can be regressed using various algorithms (e.g., maximum likelihood with gradient descent, etc.). Finally, in Fig. 1(d), the path loss prediction can be made based on the regressed model parameters.

III. Model Application

In this section, we apply the AMPLE model to two simulated outdoor scenarios: Scenario A for parameter extraction and Scenario B for model validation. We first introduce the two scenarios simulated by Ranplan Professional, along with basic information of radio propagation. Then, we describe the method for regressing the parameters of the AMPLE model under the simulation of Scenario A.

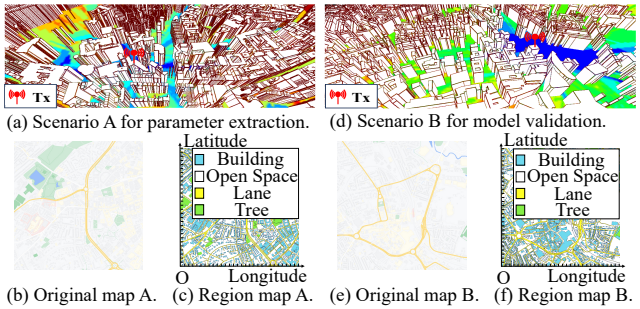

(a) Scenario A for parameter extraction. (d) Scenario B for model validation.
(b) Original map A. (c) Region map A. (e) Original map B. (f) Region map B.

Fig. 2. Two simulations with the same propagation conditions, along with environment recognition.

A. Outdoor Simulation and Environment Recognition

To validate the AMPLE model, we employ Ranplan Professional to simulate radio propagation in two outdoor scenarios for parameter extraction and model validation. For Ranplan Professional [5]–[7], it is developed by Ranplan Wireless as a commercial ray tracing simulator, which supports propagation simulations for both the indoor and outdoor environment, and has been used as validations for model characterizations in several works [23]–[25].

The simulated outdoor scenarios involve two suburban cities in the U.K.: Sheffield (Scenario A) for parameter extraction and Barnsley (Scenario B) for model validation. Detailed environment features (e.g., buildings, trees, etc.) are imported from EDINA's Digimap Ordnance Survey [26], [27] to reveal the real outdoor information in two cities, as illustrated in Fig. 2(a) and Fig. 2(d), respectively. Both simulation resolutions are set to 5 m, and the regions of the same type (e.g., buildings) are assumed to have consistent material properties. For the scenario of parameter extraction (i.e., Scenario A), it is bounded by latitudes and longitudes ranging from 53.373579 to 53.387172, and -1.49688 to -1.47412, respectively. The Tx, positioned at a height of 80 m above ground, is located beyond the rooftop of a building at coordinates (53.381029, -1.4864733). Also, the Tx is equipped with an omnidirectional antenna transmitting at Long Range Wide Area Network (LoRaWAN) 868 MHz [28], and the Tx power is 20 dBm, along with 0 dBi antenna gains for both Tx and Rx. For the scenario of model validation (i.e., Scenario B), it is bounded by latitudes and longitudes ranging from 53.548515 to 53.561859, and -1.490611 to -1.467880, respectively. Similar propagation conditions are deployed in Scenario B. Once all the propagation parameters are configured, the path loss across two simulated areas is calculated at 5-m intervals, with an Rx height of 1 m. A total of 91,596 data points for Scenario A and 89,441 data points for Scenario B are respectively collected via simulations, which are nearly 30-fold than the measurement we previously made [21], and without path loss truncation caused by device sensitivity.

For environment recognition, the square maps of Scenarios A and B are collected from Google Maps with a 50-m map scale, and the area of each scenario is about 2.25 km^2, as shown in Fig. 2(b) and Fig. 2(e), respectively. The map is then classified as *Building, Open Space, Lane*, and *Tree* using k-means clustering with manual region type combinations, and each region type is assigned with a PLE. By using the latitude and longitude boundaries, simulation results can be mapped onto the region map based on the corresponding coordinates (as shown in Fig 2(c) and Fig. 2(f), respectively), allowing for the generation of direct path matrix $\mathbf{S}_z$ for each Tx-Rx pair.

B. Parameter Regression

We consider the maximum likelihood to regress the parameters contained in (3), and the probability density function (PDF) of the zth Tx-Rx pair path loss in (3) can be written as

$$P(l_z;\mu(A,n_m,X),\sigma)=\frac{1}{\sqrt{2\pi}\sigma}\exp\Big(-\frac{(l_z-\mu(A,n_m,X))^2}{2\sigma^2}\Big), \quad (5)$$

where l_z is the zth Tx-Rx pair path loss for Z samples (i.e., $Z=$ 91,596) in total, and $\mu(A,n_m,X)$ is the mean path loss value, which is expressed in (4). The likelihood function can be computed as

$$L(\mu(A,n_m,X),\sigma)=\prod_{z=1}^{Z}\frac{1}{\sqrt{2\pi}\sigma}\exp\Big(-\frac{(l_z-\mu(A,n_m,X))^2}{2\sigma^2}\Big). \quad (6)$$

Then, the partial derivatives under natural logarithm of (6) are computed for all parameters in (3), including intercept A, PLEs n_m, building penetration loss X, and standard deviation σ, as

$$-\frac{\partial \ln L(\mu(A,n_m,X),\sigma)}{\partial A}=\sum_{z=1}^{Z}\Big(\frac{\mu(A,n_m,X)-l_z}{\sigma^2}\Big), \quad (7)$$

$$-\frac{\partial \ln L(\mu(A,n_m,X),\sigma)}{\partial n_m}=\sum_{z=1}^{Z}\Big(\frac{(\mu(A,n_m,X)-l_z)D_m}{\sigma^2}\Big), \quad (8)$$

$$-\frac{\partial \ln L(\mu(A,n_m,X),\sigma)}{\partial X}=\sum_{z=1}^{Z}\Big(\frac{(\mu(A,n_m,X)-l_z)p_z}{\sigma^2}\Big), \quad (9)$$

$$-\frac{\partial \ln L(\mu(A,n_m,X),\sigma)}{\partial \sigma}=\sum_{z=1}^{Z}\Big(\frac{1}{\sigma}-\frac{(l_z-\mu(A,n_m,X))^2}{\sigma^3}\Big). \quad (10)$$

Following (7)-(10), those parameters can be regressed together by gradient descent, which is omitted here.

IV. Results and Analysis

Based on the ray-tracing simulation of Ranplan Professional in Scenario A, we regress the AMPLE model following (7)-(10), and apply it to the simulation results of Scenario B for fair validation. We then compare its performance with the ABG model in 5GCMSIG under the urban macrocell (UMa) scenario case [18, Table6], and the 3GPP model for UMa scenario as well [17, Table 7.4.1-1].

For the prediction results, the heat maps of three models in comparison with the simulation in Scenario B are shown in Fig. 3. Note that the error maps in Fig. 3(e), Fig. 3(f), and Fig. 3(g) represent the absolute error between the model prediction results and simulation in Scenario B, which is computed as $|l_o(x,y)-\hat{l_o}(x,y)|$, where $l_o(x,y)$ and $\hat{l_o}(x,y)$ denote the simulation in Scenario B and the model predictions at the spatial point (x,y), respectively. Throughout the three error maps, the AMPLE model demonstrates better prediction performance, especially compared to the 3GPP-UMa model. The three models show similar predictions when the Rxs are close to the Tx. However, as the Tx-Rx separation distances increase, the impact of environmental complexities significantly interferes with the predictions of path loss models that do not account for these factors. These interferences are evident in

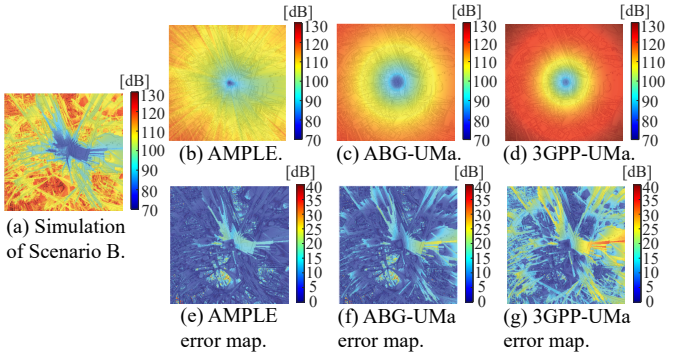

Fig. 3. Comparison of path loss heat maps under the simulated area, with the error maps depicting the absolute errors between the three models and Ranplan Professional simulation.

both the ABG-UMa and 3GPP-UMa models but are effectively mitigated by the AMPLE model.

To provide a more intuitive comparison along with the model complexity, we compute the mean absolute error (MAE) and the root mean square error (RMSE) of the three models in decibels with respect to 89,441 simulation data points using the same computer, as shown in Table I. All three models are run 10 times to compute the mean simulation time on a typical office computer (central processing unit (CPU): Intel (R) Core (TM) i5-10505 3.20 GHz; random-access memory (RAM): 16.0 GB 2133 MHz) with MATLAB-R2022a programming environment. Moreover, we draw the cumulative distribution functions (CDFs) to visualize the absolute error between the path loss models and simulation results, which are shown in Fig. 4. Overall, the path loss prediction of the AMPLE model outperforms the ABG-UMa and 3GPP-UMa path loss models.

TABLE I
PERFORMANCE OF MODELS

Model	MAE [dB]	RMSE [dB]	Mean Simulation Time [s]
AMPLE	5.75	7.43	0.136
ABG-UMa	7.20	8.80	0.138
3GPP-UMa	12.84	14.51	0.228

V. DISCUSSION

A. Why the AMPLE Model?

The real-world radio propagation involves multiple mechanisms, including reflection, diffraction, scattering, and penetration. Instead of directly revealing those mechanisms like ray-based models, those mechanisms can be alternatively modeled from their root causes — the environments that produce these mechanisms. This is reasonable since different environment types have their preferences for various mechanisms (e.g., foliage causes dense scattering, while tunnels lead to waveguide effects). Therefore, we link the environments with PLEs through digital maps to reveal the influences of multiple environmental regions on a single link. We then weight their influences individually based on the weighted distance of the direct path [21], [22]. In other words, the direct path in the AMPLE model is to reveal the environment-weighted-distance relationship. Once the parameters are regressed, the AMPLE model enables rapid deployments, while the characterization of environments via PLEs enhances its accuracy compared to other empirical models. In the meantime, similar to the

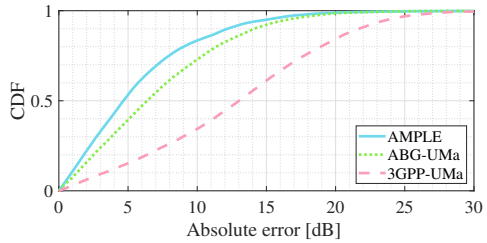

Fig. 4. CDF of absolute error between three predictions (i.e., the AMPLE, ABG-UMa and 3GPP-UMa models) and Ranplan Professional simulation.

ABG model, the formation of the AMPLE model with different parameter sets can be deployed in the corresponding scenarios, such as, urban, suburban, and rural areas. Beyond that, the AMPLE model is further adaptive to environmental complexities by adjusting the corresponding PLE numbers.

Ideally, this model can be either supported by a digital map system, or, integrated into the digital map system as a new map attribution. With the fully extracted environment information from digital map systems, the AMPLE model could achieve near real-time path loss prediction even under a complex scenario (i.e., a large number of PLEs). Overall, the AMPLE model builds a bridge between fast path loss prediction and site-specific environment emulation [29].

B. Model Expansion and Refinement

To meet the requirements of current path loss modeling, which demands a balance between computational complexity and model accuracy for further radio channel modeling (e.g., small-scale parameters), we made a tradeoff between these factors. Still, with more data and/or analysis, the AMPLE model can be expanded and refined, at some cost of complexity. For example, more scenario categories could be covered via further measurements. Also, it would be further enhanced by adding factors such as antenna heights and frequencies within each PLE corresponding to region types, to cover radio propagation in 3D and more frequency bands.

For environment recognition, beyond k-means clustering which is only suitable for pre-processed maps (e.g., Google Maps, Bing Maps, etc.), deep-learning methods such as convolutional neural networks can be considered for raw maps with arbitrary region shapes (e.g., satellite maps). Additionally, it should be noted that the environment recognition method used in this paper is a simplified approach, as the primary focus is on radio propagation. Map classification can be addressed more comprehensively as an image processing and recognition problem, which allows for more general, efficient, and in-depth solutions.

VI. CONCLUSIONS

In this letter, we introduced the AMPLE model and used the ray-tracing simulation generated by Ranplan Professional to validate the AMPLE model. Then, we compared the AMPLE model with the ABG and 3GPP models for path loss predictions. The results showed that the AMPLE model outperforms the other two models. The AMPLE model provides a new way to predict path loss with both simplicity and accuracy, and it can be further integrated with digital map systems to generate part of a digital twin channel that contains both radio propagation path loss information and map data.

REFERENCES

[1] J. Zhang *et al.*, "Channel measurement, modeling, and simulation for 6G: A Survey and tutorial," 2023, arXiv: 2305.16616. [Online]. Available: https://arxiv.org/abs/2305.16616

[2] C.-X. Wang *et al.*, "6G wireless channel measurements and models: Trends and challenges," *IEEE Veh. Technol. Mag.*, vol. 15, no. 4, pp. 22–32, Dec. 2020.

[3] A. Goldsmith, *Wireless Communications*. Cambridge: Cambridge University Press, 2005.

[4] Z. Yun and M. F. Iskander, "Ray tracing for radio propagation modeling: Principles and applications," *IEEE Access*, vol. 3, pp. 1089–1100, 2015.

[5] D. He *et al.*, "The design and applications of high-performance ray-tracing simulation platform for 5G and beyond wireless communications: A tutorial," *IEEE Commun. Surveys Tuts.*, vol. 21, no. 1, pp. 10–27, 1st Quart., 2019.

[6] *Ranplan Professional*, 2024. [Online]. Available: https://www.ranplanwireless.com/gb/products/professional/

[7] W. Yang *et al.*, "Indoor measurement based verification of ray launching algorithm at the Ka-band," in *Proc. XXXIIIrd General Assembly and Scientific Symposium of the International Union of Radio Science*, 2020, pp. 1-4.

[8] V. Erceg *et al.*, "An empirically based path loss model for wireless channels in suburban environments," *IEEE J. Sel. Areas Commun.*, vol. 17, no. 7, pp. 1205–1211, July 1999.

[9] V. S. Abhayawardhana *et al.*, "Comparison of empirical propagation path loss models for fixed wireless access systems," in *Proc. IEEE Veh. Tech. Conf.*, 2005, pp. 73–77.

[10] S. Jaeckel *et al.*, *QuaDRiGa—Quasi deterministic radio channel generator, user manual and documentation, V2.0.0*, 2017. [Online]. Available: https://quadriga-channel-model.de

[11] V. Nurmela *et al*., *METIS channel models, Deliverable D1.4,* 2015. [Online]. Available: https://www.researchgate.net/publication/282807948

[12] P. Kyösti *et al.*, *WINNER II Channel Models, D1.1.2 V1.0*, 2007. [Online]. Available: http://www.signal.uu.se/Publications/WINNER/WIN2D112.pdf

[13] M. Peter *et al*., *Measurement campaigns and initial channel models for preferred suitable frequency ranges, Deliverable D2.1,* 2016. [Online]. Available: https://ec.europa.eu/research/participants/documents/downloadPublic?documentIds=080166e5a7a6b182&appId=PPGMS

[14] S. Wu *et al.*, "A general 3-D non-stationary 5G wireless channel model," *IEEE Trans. Commun.*, vol. 66, no. 7, pp. 3065-3078, July 2018.

[15] ITU-R SG05, *Draft new report ITU-R m. [IMT-2020.eval]*, 2017. [Online]. Available: https://www.itu.int/md/R15-SG05-C-0057/en

[16] L. Liu *et al.*, "The COST 2100 MIMO channel model," *IEEE Wireless Commun. Mag.*, vol. 19, no. 6, pp. 92–99, Dec. 2012.

[17] 3GPP, *Study on channel model for frequencies from 0.5 to 100 GHz, V16.1.0*, 2020. [Online]. Available: https://www.etsi.org

[18] NTT Docomo *et al.*, *5G channel model for bands up to 100 GHz, V2.0*, 2016. [Online]. Available: http://www.5gworkshops.com

[19] S. Sun *et al.*, "Propagation path loss models for 5G urban micro-and macro-cellular scenarios," in *Proc. IEEE 83rd Veh. Tech. Conf.*, 2016, pp. 1–6.

[20] S. Sun *et al.*, "Investigation of prediction accuracy, sensitivity, and parameter stability of large-scale propagation path loss models for 5G wireless communications," *IEEE Trans. Veh. Technol.*, vol. 65, no. 5, pp. 2843-2860, May 2016.

[21] L. Zhou *et al.*, "AMPLE: An adaptive multiple path loss exponent radio propagation model considering environmental factors," 2023, arXiv: 2303.12441. [Online]. Available: https://arxiv.org/abs/2303.12441

[22] J. Zhang *et al.*, "A method of fast path loss calculation considering environmental factors," WO2023214176A1, 2023. [Online]. Available: https://patents.google.com/patent/WO2023214176A1/en?oq=WO2023214176A1

[23] K. Qiu *et al.*, "Pseudo ray-tracing: Deep leaning assisted outdoor mm-wave path loss prediction," *IEEE Wireless Commun. Lett.*, vol. 11, no. 8, pp. 1699–1702, Aug. 2022.

[24] C. Qin *et al.*, "Simulation based channel hardening of cell-free massive MIMO in mm-wave," in *Proc. 2021 XXXIVth General Assembly and Scientific Symposium of the International Union of Radio Science (URSI GASS)*, 2021, pp. 1–4.

[25] S. Bakirtzis *et al.*, "EM DeepRay: An expedient, generalizable, and realistic data-driven indoor propagation model," *IEEE Trans. Antennas Propag.*, vol. 70, no. 6, pp. 4140–4154, June 2022.

[26] *Digimap.* [Online]. Available: https://digimap.edina.ac.uk

[27] Ordnance Survey (GB), OS Open Map - Local [SHAPE geospatial data], Scale 1:10000, Tiles: se, Updated: 12 October 2023, Using: EDINA Digimap Ordnance Survey Service, Downloaded: May 2024. [Online]. Available: https://digimap.edina.ac.uk

[28] B. Eric, *LoRa documentation*, 2019. [Online]. Available: https://buildmedia.readthedocs.org/media/pdf/lora/latest/lora.pdf

[29] H. Gao *et al.*, "Digital twin enabled 6G radio testing: Concepts, challenges and solutions," *IEEE Commun. Mag.*, vol. 61, no. 11, pp. 88-94, Nov. 2023.